Climatic and geomorphic interactions on alluvial fans in the Atacama Desert, Chile

Erik W. Haug

Thesis submitted to the faculty of the Virginia Polytechnic Institute and State University in partial fulfillment of the requirements for the degree of

Master of Science
In
Geosciences

Erin R. Kraal (Chair)
James A. Spotila (Co-chair)
Panayiotis Diplas
Kenneth Eriksson
Jacob Sewall

May 01, 2009
Blacksburg, Virginia

Keywords: alluvial fan, hyper-arid, flooding, runoff, transport, climate

Climatic and geomorphic interactions on alluvial fans in the Atacama Desert, Chile

Erik W. Haug

ABSTRACT

Alluvial fan surfaces in the Atacama Desert of northern Chile preserve evidence of recent, precipitation-driven, surface flows. Determining the hydrologic characteristics of these flows is important for understanding the effects of rare yet significant storms in the region. Flow reconstruction, runoff analysis, and comparison with climatological data yield surface activation recurrence intervals of ~1-20 years for three small fans and associated catchments proximal to Iquique and Antofagasta. Relatively short-lived and intense precipitation events (1-3 hour, > 4 mm/hr) are required to mobilize and transport the largest surface grains. Modeled discharges provide minimum constraints on the rates of precipitation that yield surface-forming flows in the hyper-arid region. The results of this study aid in understanding the evolution of various surfaces in the region. In particular, results provide a clear indication of the ability of a particular storm event --i.e., precipitation rate to activate a surface.

ACKNOWLEDGEMENTS

Funding for field research was provided in part by the National Science Foundation. BP provided additional funding for work completed during the summer of 2008. Thanks to Dr. Erin Kraal, for advising and editing, as well as making field work possible and Dr. Jacob Sewall for assistance with climate data and analysis. Thanks also to Maurits VanDijk for assistance with field surveys and fan slope analysis. I wish to thank colleagues at Utrecht University: Dr. Poppe DeBoer and Dario Ventra, for their guidance and assistance in the field. I am additionally grateful for Nathalia Fouquet's help in the field and Dr. Panos Diplas's assistance with one dimensional flow modeling. Thanks also to Dr. James Spotila, who advised various aspects of the project including runoff modeling and Dr. Kenneth Eriksson for feedback and review throughout the project.

TABLE OF CONTENTS

LIST OF FIGURES

LIST OF TABLES

1 Introduction

1.1 Purpose

Regional hydrologic conditions control the rate and methods by which environments geomorphically evolve. Determining the effective hydrologic conditions --e.g., storm frequency, magnitude, and length, that promote landscape modification therefore is fundamental to developing models for understanding the way in which surfaces develop in a range of geologic and climatic settings. Quantifying the geomorphic effects of storm events is often difficult due to human environmental impacts and the lack of robust climatological data throughout the Holocene.

The Atacama Desert of northern Chile (Fig. 1) provides a unique environment to study undisturbed and undeveloped landscapes under hyper-arid conditions. The desert has experienced a sustained, arid to hyper-arid climate since > 10-15 Ma (Dunai et al., 2005; Houston, 2006b; Nishiizumi et al., 2005). Despite recent efforts to date the ages of a variety of geomorphic surfaces, the rates of creation and modification of much of the desert's surfaces are largely unknown (Clarke, 2006; Evenstar et al., 2009; Nishiizumi et al., 2005). Since the hyper-arid climate is characterized by infrequent and relatively low-volume precipitation events, understanding the role of these storms is valuable for expanding our understanding of the relationships between sediment transport and climatic forcing.

This study uses one-dimensional sediment transport modeling to determine the flows required to transport the largest clast sizes (d_{95}) on three alluvial fans and their associated catchment channels to estimate the minimum hydrologic conditions required for surface activation. Using the results of flow modeling, we explore the precipitation rates needed to

produce significant transport and examine the associated climatic implications. The results of this study can be used to predict the effects of regional storm events of varying magnitude, discuss linking geomorphic and climatic forcings in data poor environments, and examine the interactions between climate and landscape development and evolution.

2 Regional setting

2.1 Physiography and tectonics

The Atacama Desert is located along the western coast of South America extending from Peru to northern Chile (~10-27°S) (Fig. 1). The desert is formed by a series of N-S trending cordilleras and valleys from west to east. Most of the coast has a negligible coastal plain that is ~40 km at its widest. The Coastal Cordillera is the first significant mountain range with elevations averaging ~1000 m that drop steeply into the Pacific to the west. The eastern flank of the range has a gentler slope that is cut by multiple strands of the extensive NNE-SSW striking Atacama Fault System (AFS). From the Mejillones Peninsula, the Coastal Cordillera narrows towards Antofagasta.

The Coastal Cordillera terminates into a broad, longitudinally extensive valley that is covered by thick packages of alluvium called the Central Depression. The valley is characterized by large, low-angle alluvial fans that converge onto extensive pediment and pediplain surfaces. Extensive ephemeral, dendritic drainages join axial channels at valley centers particularly to the north and east. To the east, the Central Depression is separated from the second significant range known as the Pre-Andes (Pre-Cordillera) by the Domeyko Fault system. The Pre-Andes are separated from the High Andes by a second valley system characterized by longitudinally extensive evaporitic basins (salars) filled with thick playa and salt rich deposits. To the east rise

the High Andes composed of conical stratovolcanoes perched atop the Altiplano – a high altitude plateau that extends into Argentina and Bolivia to the east.

Paleotectonic reconstructions for plate motion between the Nazca and South American plates have shown a sustained subduction since prior to the late-Cretaceous (Pardocasas and Molnar, 1987). South America has maintained a broadly north-south continental trend since the late-Triassic which has contributed to the relative stasis of climate along the western coast of South America. Phases of rapid subduction and associated uplift (plate convergence > 100 mm/yr) occurred between 50 and 42 Ma and since 26 Ma (Pardocasas and Molnar, 1987).

The Atacama Fault System (AFS) has controlled the geomorphology of the Coastal Cordillera since the early-Miocene (Riquelme et al., 2003). Differential rates of uplift combined with marked periods of wetter conditions aided in the ability of rivers proximal to the AFS to erode. Current rates of vertical slip along the fault approximate 0.01 mm/yr (Gonzalez et al., 2006).

Alluvial surfaces have been used to produce estimates of the age of aridity. Quartz exposure ages using ^{21}Ne for fan surficial material suggest erosion rates of ~0.1 m/Myr with the oldest surface clast dated to be ~9 Ma (Nishiizumi et al., 2005). Other alluvial surfaces show ages of up to ~25 Ma (Dunai et al., 2005). These ages suggest that since deposition, these fan surfaces have become relict, stable features. Since the onset of hyper-aridity, steep mountainous bedrock surfaces erode more quickly than these fan surfaces due to the lack of precipitation to transport material (Nishiizumi et al., 2005). Hartley et al. (2005) claim that fans along the Coastal Cordillera have not been active for ~230,000 years and probably since the Neogene based on cosmogenic and luminescence dating. Derived denudation rates (<0.1 m/My) for the Coastal

Cordillera suggest that the area is "inactive" and may be approaching a geomorphic steady state (Kober et al., 2007). These large estimates of age for most recent activity and surface exposure have implications for the role of flooding events and the ability of climatic conditions to control material transport on alluvial fans.

2.2 Climate

The hyper-arid climate along the western coast of South America is formed by the confluence of a sub-tropical high-pressure zone that is unaffected by winter cyclonic precipitation, upwelling of cold Pacific waters related to Humboldt circulation, offshore winds, and a topographic impediment created by the High Andes that separates west-flowing Atacaman and east-flowing Amazonian/Paranan drainages (Bobst et al., 2001; Clarke, 2006). Paleogeographic reconstructions show that the South American plate has maintained Nazca plate subduction forming the N-S trending Andes, since the Cretaceous (Pardocasas and Molnar, 1987). This unique combination of geographic, hydrologic, and climatic forcing has allowed for sustained hyper-arid conditions in the Atacama Desert making it the driest desert on Earth (Clarke, 2006).

The extensive rain shadow created by the High Andes produces a rapid decrease in rainfall to the west (Houston, 2002). Between 18-24°S latitude, mean annual rainfall (MAR) is related to altitude (A) by the following equation: MAR = exp0.0012A for areas 2000-5000 m above sea level (Houston, 2002). Much of the desert, therefore, cannot maintain vegetation –with some areas unable to support any form of microbial life (McKay, 2003). Austral summer (December-March) easterly winds move relatively moist air over the Andes and precipitation falls on the Altiplano; however, much of the Atacama Desert is located outside of the extent of this

precipitation (Bobst et al., 2001). Ephemeral and perennial streams drain westward from the Andes that greatly control runoff vs. subsurface flow (Houston, 2006a).

Precipitation is also limited by the Humboldt (Peru) Current, which controls the upwelling of cold Pacific waters along the coast of Northern Chile aseasonally (Thiel et al., 2007). The Humboldt system forms a north-flowing current along the coast of Chile that was initiated by the early Tertiary (Keller et al., 1997). Though the exact timing has been debated, global climate change in the Neogene, that was unrelated to changes in Andean uplift or the Humboldt system, caused the onset of hyper-aridity (Hartley and Chong, 2002).

Fluctuations in the Quaternary climate have occurred (Bobst et al., 2001). Paleoclimate reconstructions from salt-core data show that the Pleistocene was marked by wetter periods in which expanded mud flats and saline lakes were formed between 75.7-60.7 ka and 53.4-15.3 ka. During the Holocene, shorter, "wet" conditions between 11.4-10.2 ka and 6.2-3.5 ka occurred. These wetter periods correspond to insolation maxima; however, other, unknown controls exist that affect precipitation in the Atacama (Bobst et al., 2001). Grosjean et al. (2001) attribute paleo-lake transgression during the late Pleistocene to Atlantic sourced effective moisture. Palynological records from Laguna Miscanti (~23°S) agree with terrigenous sediment records to the south that indicate a sustained arid climate since ~8 ka (Grosjean et al., 2001). Historical precipitation data are sparse and incomplete. At present, annual precipitation averages ~5 mm and is delivered primarily by a coastal fog (camanchaca), with increasing precipitation to the east (Hartley, 2005).

Paleoclimate reconstructions for the mid-Chilean latitudes (~30-37°S) show more radical changes within the past ~28,000 years than in the Atacama (Lamy et al., 1999). South of the

Atacama, sediment core data from the continental shelf provide evidence of high sedimentation rates and an overall wetter climate from 18-28 ka with increasing aridity and lower sedimentation and chemical weathering since 18 ka. The wetter climate occurred synonymous with deglaciation. Lamy et al. (1999) argue that shifts in the latitude of the Westerlies strongly controls the climate in central Chile, and that those changes are preserved in terrigenous sediment deposited on the continental shelf of Chile. Northerly shifts of the Westerlies during the Last Glacial Maximum, as well as shorter-term shifts since LGM, contribute to the sustained climatic conditions in north-central Chile today.

2.3 Alluvial fans

The abundant fans in the Coastal Cordillera and Central Depression of the Atacama Desert record past sediment transport (Fig. 1). Alluvial fans form semi-conical lobate wedges of clastic sediment as steep mountainous catchments emerge onto lowland adjoining valleys (Blair and McPherson, 1994). These geomorphic features have been well studied since the mid-seventeen hundreds –e.g., see Blair and McPherson (1994) for review of alluvial fan research, and are important for understanding the past and active processes of sedimentation. Alluvial fans can form in both humid and arid environments. Blair and McPherson (1994) delineate two major types of fans: 1) debris flow process dominated and 2) fluvial, or sheet flood process dominated. More recent workers have focused on the complexity of processes and interactions between styles of deposition on fan surfaces –e.g., (Blair, 1999); (Stock et al., 2008); (Milana and Ruzycki, 1999), etc.

The processes that control fan morphology are complex and include interactions between uplift, subsidence, climate, depositional processes, and lithology (Blair and McPherson, 1994;

Densmore et al., 2007). Alluvial fans commonly form in regions of active uplift where normal-faulted footwall blocks form catchments and material is deposited onto subsiding down-thrown hanging wall blocks. In such circumstances, the rates of relative uplift control the aggradational, back-stepping, or progradational rates and history. In other cases, however, a change in climatic forcing may exert the strongest control on fan slope and morphology. Densmore (2007) found that sediment transport efficiency controls the long profile slope of fans rather than the dominance of debris flow or fluvial activity. One uniting observation is that fans have distinct spatial variation. Hooke (1965) noted that varying discharge causes deposition in discrete sections of the fan, thus creating differential slopes and morphologies on the same fan apron. Discrete depositional segments are often delineated by breaks on debris flow dominated fans (Blair and McPherson, 1998).

Alluvial fan morphometrics can be used to determine the processes associated with the formation of an alluvial fan. The ratio of fan area to fan catchment area can be used to indicate formative processes --e.g., see Hooke, (1979); Blair and McPherson, (1994). In general, steeper fans (~5-15°) are formed by debris flow processes; whereas gentler sloping fan surfaces (~2-6°) are formed by fluvial processes. The ability of a fan to transport the gravel fraction of sediment diminishes exponentially (Stock et al., 2008). Local relief across a fan surface is greater on fans that are constructed by debris flows than by a combination of fluvial and debris flows (Volker et al., 2007). The fan surface drainage density, rarity of interfluves, and erosional terraces can be used to determine the most recent active processes. These characteristics can be analyzed using high-resolution spatial data including aerial photography and LIDAR or DGPS derived DEM data, etc. Thus, sedimentological characteristics are intimately tied to morphometrics, including

slope, fan area, and depositional processes.

Multiple approaches for modeling the formation and morphometry of alluvial fans have been proposed. Controls on fan development can aid understanding the processes that transport sediment in closed systems. Finite difference modeling has been used to determine risks associated with mud and debris flows on alluvial fans (O'Brien et al., 1993; Pelletier et al., 2005). These models utilize digital elevation models to determine flows and spatial hazard. Parker et al. (1998) use one dimensional modeling to show that the concavity or convexity of fan profiles indicates the type of sediment transport active on fluvial fans --i.e., bed-load vs. suspended sediment. Furthermore, they show an inverse relationship between the amount of water discharged over a fan and the slope of that fan. More complex modeling in two or three dimensions can provide increasingly precise predictions of erosion and accumulation of fan surfaces. This study uses a one-dimensional model for the purpose of determining the conditions under which fans form rather than the morphometrics resultant from known flows.

3 Materials and methods

3.1 One-dimensional flow modeling

3.1.1 Approach

The goal of this analysis is to determine the minimum hydrologic conditions under which large (~d_{90}-d_{95}) surfaces clasts are transported for small alluvial fans and associated catchments located proximally to Iquique and Antofagasta, Chile (Fig. 1B; 2). Due to the persistent ephemeral conditions for these systems, direct measurements of flow properties are not possible. Available historical data are greatly limited in spatial resolution and precision. Thus, we utilize a

modified version of Costa's analysis to reconstruct paleo-flows that does not rely on stream gauging techniques (Costa, 1983).

This approach is limited by the preservation of the examined surfaces. Eolian influences, such as millimeter to centimeter scale ripples of silt and sand, as well as accumulations of sand downwind of micro-topographic features and on distal areas of fans where channelization and lobe deposits were noted, are observed on fan surfaces. Particles transported by eolian processes were coarse sand and smaller. Therefore, we must rely on the $d_{90\text{-}95}$ to record the competence of flows and acknowledge that secondary modification of the alluvial surface is possible and observed. Additional error may be introduced by our sampling technique --which approximates the d_{95} within a one-meter radius by visual inspection. We are confident that we have selected the largest particle in each area measurement; however, the particle may not statistically represent the d95 in all cases if significantly larger material has been buried during a single storm event.

3.1.2 Data collection

Three alluvial fans and associated catchments were surveyed using a Real-Time Kinematic Differential GPS (DGPS) system (Fig. 2 A, C). DGPS position and elevation (a.s.l.) were recorded every 0.25 m where accuracy was known to be ± 0.05 cm in three-dimensional space (Fig 3). Additional error (± 1 cm) in elevation was introduced by variation associated with the rover backpack height above ground during survey. Measurements of sediment grain size were measured to the nearest millimeter and correlated with position along profile and slope every ~10-20 m, as well as when significant change in grain size distribution were notable. The largest visible particle (d_{95}) was measured by examining the area within a one-meter radius for the

largest surface clast. The "mode" grain size (d_{md}) was recorded in a similar manner by estimating the *most common* grain size within a one-meter radius by visual inspection.

Elevations collected in the field were checked for accuracy by comparison to Digital Elevation Models generated from Advanced Spaceborne Thermal Emission and Reflection Radiometer (ASTER) derived data with a resolution of 30 m. Using the 3D analyst, elevations along channels and fans were extracted. While differences in absolute elevation occur between surveyed and DEM data (±25 m), average slopes derived from these data sources compare well.

3.1.3 Model explanation

Developing equations and predictive models for sediment movement and associated flows has long been a difficult task in environmental engineering, hydrology, and geomorphology. Many studies have worked to form empirical equations from field and experimental data. Much of the pioneering work in sediment transport occurred during the late 1950s-70s for alluvial, sandy streams. However, since rivers are complex systems that form longitudinal profiles from steep headwater catchments to base level, grain sizes will often vary by orders of magnitude. Hack (1957) identified a relationship between slope, grain size, and drainage area for streams located in Virginia and Maryland with grain sizes between 5-600 mm. Since grain size is an important controlling factor for sediment transport, recent research has focused on understanding gravel and boulder bed river systems.

Many approaches exist for predicting sediment discharge in rivers (Chang, 1988). Bed load transport formulas rely on steady, uniform flow conditions with non-cohesive sediment. Two main approaches are used to describe the transport of bed material in a flow: the shear stress and power approaches. Shear stress is the tractive force per unit area applied to the channel

boundary on which the bed load moves by sliding or rolling (Chang, 1988). DuBoys (1879) was the first to develop an equation for the critical shear stress (stress required at incipient particle motion) that utilized the concept that bed-parallel layers of sediment moved at different speeds due to differential stresses acting on them at varying depths. Shields (1936) developed a universal, dimensionless formula that, in principle, states that the excess shear stress is available to move sediment. More recent work utilizes the equal mobility concept --e.g., see (Parker, 1982); (Diplas, 1987), in which the bed has a coarse upper layer that renders all surface particles equally capable of being entrained by a given flow.

The accuracy of estimating flows from gravel and boulder bed grain sizes has been a topic of recent debate. Costa (1983) tested the accuracy of paleohydraulic reconstruction of flash flooding by examining boulder deposits in nine basins along the Colorado Front Range. Costa's work integrated multiple methods --e.g., (Baker and Ritter, 1975); (Bradley and Mears, 1980), for determining flow depth and channel bed velocities. Costa recognized that other methods underestimate slope-area discharge for small streams and demonstrated that large boulders (~d_{90} – d_{95}) can be used to reconstruct paleovelocity and depth for small (< 30 km^2) basins. Wilcock (2001) criticizes methods for estimating bed-load transport rates using sampled material only and instead proposes a calibrated model that utilizes a measured transport rate. Unfortunately, this is not possible for ephemeral or dry streambeds, where sampling and measurements of slope, width, etc. are the only proxy by which paleo-flows can be estimated. Andrews (2000) showed that streams with a large range of grain sizes are significantly affected by the large particles on the bed that exert a strong drag on the flow. Therefore, a single estimate of grain size cannot be

used to estimate skin friction for a given channel. Rather, reach averaged values for a range of grain sizes must be used.

This model utilizes a modified version of the approach of Costa (1983) for reconstruction of flash floods in boulder streams in the Front Range in Colorado. The set of methods and equations outlined herein provides both an empirical and theoretical estimates for the minimum flow conditions --i.e., velocity, depth, and discharge, required to initiate motion of the largest particles at the surface. The major assumptions that underlie this analysis are: 1) material is transported under a fluvial regime –i.e., the ratio of volume of water to sediment is high, 2) the particles behave as non-cohesive sediment, 3) the coarsest particles measured at the surface provide a good indication of the largest load moved by a storm event, and 4) using the mean of multiple methods provides the most accurate estimate for determining flow conditions under which the current surface formed.

In this study, observations of simple v-shaped channels with steep slopes suggest that catchment channels behave as fluvial chutes that transport sediment onto fan surfaces at high velocities. The coarsest material in each system is located proximally to the fan apex, which acts as a trap as the confined channel exits the catchment onto a lower-sloped fan surface. Imbrication and channelization suggest that upper fans behave as a fluvial system, in contrast to lower fan aprons which show some evidence of transition to critical or debris flows with discreet lobes ~1 meter long and a few centimeters in height. Due to the complexity of modeling debris flows and the quality of available data, we focus only on the deposits that are believed to have formed in a fluvial regime.

The coarsest particles located at the surface record the largest material transported by the most recent storm or storms. This assumption is limited by the availability of sediment in the system. For example, if catchment bedrock is densely fractured before it is dislodged from the catchment walls, the fans may record an apparent flow competence as a given storm may have been able to transport larger material in a non-detachment limited system. Large (~0.5-1 m) angular bedrock blocks were exposed in and above the catchment channel and were available for transport. Fractured bedrock is present in each catchment and provides a range of coarse material for transport.

To reconstruct the minimum velocities required to entrain the coarsest particles on the fan surfaces and in catchment channels, one theoretical and three empirical methods were used. The methods chosen were based on the work of Costa (1983). The equations and variables used are summarized in Table 2.

Costa (1983) uses a simplified form of the theoretical relationship between drag, lift, gravitational, and frictional forces required for incipient motion developed by Bradley and Mears (1980): $v_b = [2 (\gamma_s - \gamma_f) d_I g \mu / \gamma_f (C_L + C_D)]^{0.5}$, where v_b is velocity (m/s) just above the stream bed, $\gamma_{s,f}$ are the specific weights (N/m^3) of the sediment and fluid respectively, d_I is the intermediate particle diameter of the d_{95}, g is the gravitational acceleration (m/s^2), μ is the coefficient of static friction, and $C_{L,D}$ represent lift and drag coefficients respectively. This relationship is based on the assumption that fluid and drag forces equal the gravitational and frictional forces at incipient motion --i.e., particle rolling and sliding. Similarly to Costa, we assume fluid specific weight to be 9800 N/m^3. This number cannot be directly measured since suspended sediment will influence the density of the flow. Stelczer (1981) suggests that fluid

density is not a significant factor in bed-load transport. Sediment specific weight was assumed to be 25970 N/m^3 since bedrock and derived d_{95} particles are composed of porphyritic andesite. The coefficient of static friction was assumed to be 0.7 after Costa (1983) and the U.S. Bureau of Reclamation's analysis of large crushed rock. Equations referencing d_I assume cubic boulders, which, while not exact, are approximate.

The empirical methods to determine minimum velocity utilize functions that are derived from a variety of field observations that relate flow properties to particle size. A least squares regression through 123 measurements of particles larger than 50 mm yields the following equation: $v_b = 0.20\ d_I^{0.455}$. Most of the data regressed are between 50 and 500 mm in diameter, which closely match the particle sizes of d_{95} for this study. A riprap stability derived equation from U.S. Bureau of Reclamation data yields: $v_b = 5.9\sqrt{d_I}$ (Costa, 1983; Strand, 1973). The data used in this regression originate from extensive testing for limiting sizes of riprap clasts to provide stable banks in rivers. The final method is the best fit to the least squares regression of the mean of four methods used by Costa (1983): $v_b = 0.18\ d_I^{0.487}$. The equation uses particles between 50 and 3200 mm in diameter.

Bed velocity is related to the depth averaged flow velocity (v) by the following equation: $v = \sim 1.2\ v_b$ for channels of this type (Baker and Ritter, 1975; Costa, 1983; Strand, 1973). The results from these calculations were averaged (Table 1) and shown in Figure 3C.

Reconstructing depths associated with minimum flow velocities requires the average flow velocities calculated above as well as slope as inputs to determine associated minimum depth. Following Costa (1983), four methods are used to reconstruct paleo-flood minimum depth.

The simplest method requires rearrangement of the well used Manning's equation solving for depth: $D = [(v\ n)/S^{0.5}]^{1.5}$, where v is depth averaged velocity from the previous calculations, n is assumed to be 0.05 since the channel is rough, and slope (S) was determined from field GPS data: $S = |(h_2-h_1)/(d_2-d_1)|$, where $h_{1,2}$ and $d_{1,2}$ are consecutively measured elevations and distances respectively. Second, the concept of unit stream power (ω), as defined by Bagnold (1966) allows for the rearrangement to solve for depth: $D = \omega/\gamma_f\ S\ v$. Unit stream power is related to particle size for coarse material by the following: $0.009\ d_i^{1.686}$ (Costa, 1983). Third, a modified form of Shield's equation was evaluated for depth: $D = [\tau^*\ d_I(\gamma_s - \gamma_f)]/(\gamma_f S)$, where $\tau^* = \tau/[d_I\ (\gamma_s-\gamma_f)]$ and τ is the shear stress associated with coarse particle motion: $0.163\ d_I^{1.213}$ (Costa, 1983). The final approach for reconstructing depth combines the Darcy-Weisbach friction factor ($f = 8\ g\ D\ S/v^2$) with the work of Limerinos which relates friction to relative smoothness: $1/\sqrt{f} = 1.16 + 2.03 \log (D/d_I)$ (Costa, 1983; Limerinos, 1970). Limerinos' equation was developed for coarse particles up to 500 mm, which is consistent with particle sizes in our dataset. The arithmetic mean of these four methods is reported in Table 1C and shown in Figure 5.

The reconstructed velocities and depths can be used to calculate associated discharges if the channel cross-section is known. Cross-sectional area can easily be determined as the catchment channels are simple v-shaped culverts and require only a transverse slope to be known: $A = 0.5\ D/\tan(S_T)$, where A is cross-sectional area and S_T is the slope perpendicular to the direction to stream flow. Using these areas and velocities, discharge can be calculated: $Q = vA$ (Table 1C).

3.2 Runoff analysis

The WinTR-55 model is a well-accepted method for small watershed hydrology that calculates theoretical runoff produced from a single-event according to known and/or estimated values for

the geomorphic variables of an area (USDA, 1986). This model is based on previous efforts by the USDA Soil Conservation Service (SCS) to quantify storm runoff, peak discharge, and hydrographs for agricultural and urban water management. For a complete discussion of the model theory see the WinTR-55 users manual (NRCS, 2005).

Inputs to WinTR-55 include the following: catchment area, hydrologic soil group, time of concentration, stream length, rainfall volume, and hydrograph type. Stream length and catchment area were known and constant for each model run. We defined the dependent variable as the precipitation volume, which was varied for each basin to determine the minimum threshold required to transport d_{95} clasts on each of the fan-catchment systems.

The minimum time for all areas of a particular basin to begin contributing runoff to the stream outlet is called Time of Concentration (T_c). WinTR-55 calculates T_c based on the stream length, slopes, average distance to stream, and flow velocity. Since these catchments have exceedingly simple and small areas, we can reasonably determine the T_c to be ~6 ± 2 min. for all three of the catchments studied.

The hydrologic soil group is related to the curve number (CN), which is a function of infiltration rate. Due to difficulties determining infiltration rate directly in the field, we must assume rates based on qualitative observations of the surfaces of study. For fan areas, we assume relatively high infiltration rates (CN = 76 --i.e., unvegetated, arid gravels). A thin (5-20 cm) veneer of highly chemically weathered sediment overlies bedrock and coarse gravels in the catchment. thus, for catchment areas, we assume slightly lower rates (CN = 72 --i.e., unvegetated, arid packed sands and gravels). The infiltration rates are weighted based on area for the model.

We assume that precipitation was delivered via normally distributed hydrographs with the model assessed for one, three, six, twelve, and twenty-four hour storm durations. These periods were chosen based on the hyper-arid climate. In other regions, aridity is typically associated with relatively short-lived and intense precipitation usually via convective cells (Almedeij, 2005). The longer storm periods --i.e., six, twelve, and twenty-four hours, were assessed to examine the effects of storms of sustained, yet lighter precipitation --e.g., rainfall associated with cyclonic activity.

3.3 Climate data

Climatological data are prone to a variety of errors and inconsistencies due to spatial and temporal resolutions. Historical climate observations --i.e., temperature, rainfall, etc., typically do not extend back in time more than one to two centuries and are limited to the mid-1600s by the development of modern thermometry and tipping bucket rain gauging. Additionally, accuracy and precision of measurements, as well as completeness of record become questionable prior to the early 1900s before the rise of modern aviation. Modern technology --e.g., satellite, doppler radar, etc. allows for greatly improved accuracy of measurement, though issues of spatial precision and resolution persist. The preponderance of data scale and quality leads to difficulty in describing the relationships between climate and geomorphic development in a particular region. To overcome these challenges, we utilize multiple datasets to determine the frequencies with which the studied alluvial fans and associated catchments are activated. Due to weaknesses inherent in each of the individual datasets, we compare the predicted recurrence intervals to minimize these.

The first dataset used for climate comparison is composed of directly observed historical records combined from Ortlieb (1995) and Vargas (2006). The dataset records individual precipitation events ±1 mm, though individual measurements may be less accurate (Fig. 4). These data are limited by the lack of precise and complete records. For example, many years have no recorded precipitation, in contrast to other datasets with multiple events. Additionally, the event duration was not recorded for most events. We assimilated data from 1904 to 2000 for this study.

NCEP/NCAR Reanalysis (National Center for Environmental Protection/National Center for Atmospheric Research) provides a globally modeled dataset that utilizes observed data to constrain the model's output according to known records (PSD, 2009). Inputs to the model include > 80 variables --e.g., geopotential height, relative humidity, temperature, convective and radiative heating, and precipitation rate (PSD, 2009). The dataset is powerful as a tool to fit a global dataset of temporal observations to a climate model. Since a purely theoretical model may reproduce various phenomena, the timing and magnitudes of those events may not be consistent with history. Thus, the NCEP/NCAR reanalysis benefits from the theoretical model that fills spatial gaps in observed data according to known variables in nearby regions and global observations. Additionally, these data provide the finest timescale with six-hourly measurements of precipitation rate (Fig. 4). Despite the relatively fine scale of measurements, the data are limited in that they cannot capture the precipitation rates for storms of shorter duration than six hours. Therefore, short-lived convective storms will not be identified in this dataset.

The Global Precipitation Climatology Project (GPCP) dataset provides monthly totals for precipitation using satellite measurements. The spatial scale of these measurements is registered

as 2.5° latitude and longitude cells. The satellite algorithms for averaging precipitation rate over a cell is presumably quite precise, though may be somewhat inaccurate for the purposes of this study since coastal and high Andean precipitation may positively affect the monthly totals. Thus, GPCP may over-estimate precipitation totals. Figure 4 shows that GPCP estimates for fan activation are above the mean of all datasets.

Willmott and Matsuura from the University of Delaware have assembled data from the Global Historical Climatology Network, as well as the archive of Legates and Willmott (Willmott, 1999). The dataset, which extends from 1950-2000 will be referred to herein as UDel (Fig. 4). The data are directly observed from weather and gauging stations on land only and reported to an accuracy of ±1 mm. The greatest advantage of this dataset comes from a spatial resolution of 0.5° latitude-longitude cell size. Unfortunately, limitations associated with the limited number and distribution of gauging stations likely cause underestimation of precipitation totals.

WinTR-55 calculated thresholds for storm runoff capable of mobilizing d_{95} surface materials can be used with the acquired climate datasets in order to quantify the number of times per dataset each system has been active. To accomplish this, each dataset was filtered for all recorded events that exceeded WinTR-55 estimates. Since each dataset covers different time periods and records at different intervals, the data were assessed only for the period 1979-2000 since they each share that coverage. NCEP/NCAR Reanalysis show that 0-1 events have occurred during a month of record. There are 12 months in the period 1979-2000 that record multiple events, but in all cases, no more than one event exceeds calculated thresholds for runoff. Thus, monthly totals can be used as a measure of precipitation on a per event basis.

4 Results

4.1 Flow reconstructions

Velocities reconstructed from particle and slope measurements indicate an average velocity of ~3 m/s as water exits the catchment of fan 1 (Fig. 3) and ~3.5-4.7 for fans 2 and 3 respectively. These high rates of flow reflect the steep slopes over which the flow is routed. We expect fan 1 to have a lower velocity since it is located near Iquique, north of fans 2 and 3, and therefore will receive, on average, lower amounts of precipitation that is capable of transporting material smaller than that found on fans 2 and 3. Since average annual precipitation decreases to the north, this is consistent with our results. The relative difference between velocities at the fan apex of fans 2 and 3 may be explained by the rapid decrease in slope up profile of the apex of fan 3 (Fig. 3). The low slope at the apex of fan 3 means that water must move significantly faster to transport the material deposited there than on fan 2. In general, velocities increase as slopes increase from the catchment boundary to the fan apex and then decrease onto the upper fan.

Depth reconstructions on fans 1-3 show that flows ~5-20 cm deep were associated with the formation present day alluvial surfaces (Fig. 5) and are consistent with field observations of shallowly channelized areas of the upper fans. Depths cannot be reconstructed for the fan surfaces since the channel forms and micro-topographic influences on flow mechanics are unknown. In general, a slight increase in flow depths is noted down-profile. This is probably due to larger material in the channels proximal to the fan apices.

Average discharges associated with the modeled flow velocities and depths are 0.081 m^3/s for fan 1 and 0.129 and 0.175 m^3/s for fans 2 and 3 respectively. These values suggest that relatively low discharges are capable of moving significant amounts of material. An axial channel ~ 1.5 m

deep and ~10 m wide flows NE cutting the toes of fans 2 and 3. The size of this channel represents the erosive power of these flows as multiple fans upstream provide water during storm events. A summary of model results is shown in Table 1C. These values are used as input thresholds for runoff analysis.

4.2 Runoff analysis and frequency

WinTR-55 results in Figure 6 show minimum thresholds to exceed discharges determined from one-dimensional flow modeling. Storms of greater duration must deliver significant volumes of precipitation in order to exceed these thresholds since modeling provides runoff estimates using a normally distributed hydrograph. For example, to activate the largest surface material on fan 1, only ~0.4 cm of precipitation is required for a storm duration of one hour, whereas a 24 hour storm must deliver ~9.5 cm for the same mobilization to occur. If we reduce the surface activating thresholds to precipitation per hour (Fig. 6), fan 1 requires the lowest rate (~4 mm/hr) to activate d_{95} and smaller particles. Fans 2 and 3 requires ~6.5 and ~8.1 mm/hr respectively (Fig. 6, Table 3).

Modeled storms are well-within the constraints of recorded events in the region and allow a first-order determination of the frequency that surface forming events occur (Fig. 7). Figure 7 shows the number of times per year that each fan is activated according to different climate datasets for the period 1979-2000. Frequency analysis was reported over this time interval since all acquired datasets cover this period (Table 3).

Fan 1 experiences significant surface forming flows more frequently (~1.3 times/year) compared to fans 2 and 3 (~0.7-1 time/year). NCEP/NCAR reanalysis provides the highest frequency for activating the fans (~1.3-2.3 times/year), whereas the Vargas and Ortlieb data

estimate the lowest frequency (~0.25-0.35 times/year). Two orders of magnitude of variance are seen amongst the datasets depending on which is used to estimate frequency. The means of these calculations are shown as grey bars.

5 Discussion

5.1 How often do surfaces activate?

Despite the hyper-arid conditions present in the region, surface activating flows occur more often than might be expected (Fig. 7). Paleo-flow reconstructions suggest that the northern system (fan 1), which was noted to have smaller d_{95} clasts than those in the south (fans 2 & 3), is activated more frequently than those areas proximal to Antofagasta (fans 2 & 3). Average annual precipitation in the north, measured at Iquique, is lower than that of Antofagasta. But since material is somewhat finer on fan 1, the threshold for surface activation is less (Fig. 3, 7) resulting in more frequent activation.

The frequencies of surface activating storms were assessed for each dataset by simply counting the number of times that each dataset exceeded the threshold for activation calculated using the WinTR-55 runoff model for Vargas/Ortlieb and NCEP/NCAR Reanalysis since they each data plot individual events (Table 3). Unfortunately, GPCP and UDel data report precipitation values as monthly totals and sum all events within a given month. This method of reporting creates difficulty in knowing whether multiple events occurred in a given month. If multiple events occurred in a month, we have over-estimated the frequency with which surfaces are activated since individual events may not have exceeded precipitation thresholds if measured individually.

NCEP/NCAR Reanalysis provides the finest timescale over which precipitation rates are reported. Examination of these rates shows that months with multiple events do not yield significant precipitation totals. Precipitation rates in months with multiple events approximate < ~0.1 mm/6 hr which are ineffective at producing significant runoff and when summed do not exceed our thresholds. Thus, we must assume that summative effects of rainfall reported as monthly totals do not affect our estimates of surface activation frequency. Unfortunately, this cannot be verified for GPCP or UDel. However, GPCP and UDel activation frequencies do fall between the range of NCEP/NCAR Reanalysis and Vargas/Ortlieb.

The studied surfaces, therefore, are activated approximately annually, and sediments with grain sizes up to ~0.5 m in diameter are capable of being transported under flows < 20 cm deep. These results reform our image of these desert surfaces into active landforms rather than fossilized static areas. Furthermore, despite experiencing the driest and longest sustained hyper-arid climate on Earth, relatively low-magnitude precipitation events are fully capable of modifying and removing coarse sediment from mountainous catchments. The relative ease and frequency with which small catchments can funnel sediment onto these fan surfaces is striking.

5.2 Reconciling climate discrepancies among datasets

The goal of compiling four separate datasets for analysis is to provide the most accurate summary of precipitation events over the past century in the Central Atacama Desert. Close examination of storm records among these data yield significant discrepancies in both timing and magnitude of precipitation.

Data from UDel and Vargas/Ortlieb are expected to compare well since they are each based on limited weather station data and gauging networks since 1950. Since the Vargas/Ortlieb data

do not provide a precise timing for each storm event, it is possible that some measurements will be listed as having occurred at a different time; however, correlative events with similar magnitudes should be visible within the UDel data. In most cases the magnitudes of storm events are significantly different in the UDel data than they are in Vargas/Ortlieb. UDel data are reported as monthly totals; thus, for months that have multiple recorded events, the UDel data will report a summed total of all precipitation, whereas Vargas/Ortlieb report only individual events --with events below a few millimeters absent in most cases. Furthermore, UDel and Vargas/Ortlieb likely under-report total precipitation since their data are collected from point sources and interpolated over larger areas.

In contrast, GPCP data utilize satellite interpolation that can provide greater accuracy of precipitation measure but at the cost of lower spatial resolution. The coarse resolution would not inherently pose a problem, though in the Atacama, precipitation has been directly correlated with elevation increase to the east (Houston, 2002). Therefore, precipitation falling east of the studied fan systems may be incorporated into the data provided in the dataset cell.

NCEP/NCAR reanalysis is expected to compare well with observed storms since the model is calculated using a multitude of observed weather and atmospheric variables. If the model is constructed accurately and adequately described inputs are supplied for the studied region, the results should output storm events that occur at roughly the correct times but with potentially differing magnitudes. Our analysis yields results indicating that NCEP/NCAR reanalysis over-estimates the precipitation for the north-central Atacama when compared to the accompanying datasets.

The wide range of timing and values for precipitation totals is therefore related to spatial, temporal, and accuracy differences among datasets. The veracity of each dataset cannot be assessed at all times, but the trends --i.e., storm event and magnitude frequency can be evaluated.

5.3 Implications for climate and geomorphology

Climate and geomorphology are intimately tied in the Atacama Desert. The unique combination of sustained hyper-aridity and lack of human modification has produced a "sandbox" in which geomorphic evolution can be examined. Results from this study show that relatively low-magnitude rainfall events are capable of entraining the largest particle sizes present in steep catchments and on small alluvial fans. Understanding the relationships between sediment transport and climatic conditions in the region --i.e., thresholds required for surface mobilization, allows for the prediction of individual storm effects.

The wide range of grain sizes available for transport and the calculated frequencies with which they are mobilized show that even under hyper-arid climatic regimes, the desert landscape will generate thick semi-continuous packages of sediment associated with trivial precipitation. The accumulation rates of sediment in these systems are directly related to the availability of sediment and the distances over which materials are transported during flow events. Determining the geomorphic effectiveness of flows in differing climates is therefore an important undertaking for further quantifying the interactions between climate and geomorphology.

6 Conclusions

Three small alluvial fans and their associated catchments in the Atacama Desert have been activated annually to semi-annually according to flow reconstructions utilizing d_{95} grain sizes

and slope measurements between 1979-2000. While average annual precipitation decreases to the north, the fan-catchment system proximal to Iquique activates more frequently than those proximal to Antofagasta.

Combining multiple climatological data while recognizing each source's strengths and weaknesses is vital to understanding the true character of precipitation in a region. Difficulty in identifying spatial and temporal records of adequate precision and accuracy make datasets less useful as individuals. According to our reconstructions, satellite data (GPCP) and amalgamated observed data (UDel) most closely approximate the mean of all data sources for surface activation frequency.

The unique geomorphology and sustained climate in the Atacama Desert warrant further study. Frequent activation of alluvial fan surfaces allows for tracing the positions of large particles to quantify the distance materials move to refine our understanding of how landscapes evolve in the hyper-arid climate.

7 References

Almedeij, J.H., Diplas, P.,, 2005, Bed load sediment transport in ephemeral and perennial gravel bed streams: EOS, Transactions American Geophysical Union, v. 86, p. 429-434.

Andrews, E.D., 2000, Bed material transport in the Virgin River, Utah: Water Resources Research, v. 36, p. 585-596.

Bagnold, R.A., 1966, An approach to the sediment transport problem from general physics: U.S. Geolocigcal Survey Professional Paper, v. 422-1, p. 37.

Baker, V.R., and Ritter, D.F., 1975, Competence of Rivers to Transport Coarse Bedload Material: Geological Society of America Bulletin, v. 86, p. 975-978.

Blair, T.C., 1999, Cause of dominance by sheetflood vs. debris-flow processes on two adjoining alluvial fans, Death Valley, California: Sedimentology, v. 46, p. 1015-1028.

Blair, T.C., and McPherson, J.G., 1994, Alluvial Fans and Their Natural Distinction from Rivers Based on Morphology, Hydraulic Processes, Sedimentary Processes, and Facies Assemblages: Journal of Sedimentary Research Section a-Sedimentary Petrology and Processes, v. 64, p. 450-489.

—, 1998, Recent debris-flow processes and resultant form and facies of the dolomite alluvial fan, Owens Valley, California: Journal of Sedimentary Research, v. 68, p. 800-818.

Bobst, A.L., Lowenstein, T.K., Jordan, T.E., Godfrey, L.V., Ku, T.L., and Luo, S.D., 2001, A 106 ka paleoclimate record from drill core of the Salar de Atacama, northern Chile: Palaeogeography Palaeoclimatology Palaeoecology, v. 173, p. 21-42.

Bradley, W.C., and Mears, A.I., 1980, Calculations of Flows Needed to Transport Coarse Fraction of Boulder Creek Alluvium at Boulder, Colorado - Summary: Geological Society of America Bulletin, v. 91, p. 135-138.

Chang, H.H., 1988, Fluvial Processes in River Engineering: Malabar, Krieger Publishing Company.

Clarke, J.D.A., 2006, Antiquity of aridity in the Chilean Atacama Desert: Geomorphology, v. 73, p. 101-114.

Costa, J.E., 1983, Paleohydraulic Reconstruction of Flash-Flood Peaks from Boulder Deposits in the Colorado Front Range: Geological Society of America Bulletin, v. 94, p. 986-1004.

Densmore, A.L., Allen, P.A., and Simpson, G., 2007, Development and response of a coupled catchment fan system under changing tectonic and climatic forcing: Journal of Geophysical Research-Earth Surface, v. 112, p. -.

Diplas, P., 1987, Bedload Transport in Gravel-Bed Streams: Journal of Hydraulic Engineering-Asce, v. 113, p. 277-292.

Duboys, P., 1879, Le Rhone et les Rivieres a Lit Affouillable: Annales des Ponts et Chaussees, v. 18, p. 141-195.

Dunai, T.J., Gonzalez-Lopez, G.A., Juez-Larre, J., and Carrizo, D., 2005, Preservation of (Early) Miocene landscapes in the Atacama Desert, northern Chile: Geochimica Et Cosmochimica Acta, v. 69, p. A161-A161.

Evenstar, L.A., Hartley, A.J., Stuart, F.M., Mather, A.E., Rice, C.M., and Chong, G., 2009, Multiphase development of the Atacama Planation Surface recorded by cosmogenic He-3

exposure ages: Implications for uplift and Cenozoic climate change in western South America: Geology, v. 37, p. 27-30.
Gonzalez, G., Dunai, T., Carrizo, D., and Allmendinger, R., 2006, Young displacements on the Atacama Fault System, northern Chile from field observations and cosmogenic Ne-21 concentrations: Tectonics, v. 25, p. -.
Grosjean, M., van Leeuwen, J.F.N., van der Knaap, W.O., Geyh, M.A., Ammann, B., Tanner, W., Messerli, B., Nunez, L.A., Valero-Garces, B.L., and Veit, H., 2001, A 22,000 C-14 year BP sediment and pollen record of climate change from Laguna Miscanti (23 degrees S), northern Chile: Global and Planetary Change, v. 28, p. 35-51.
Hack, J.T., 1957, Studies of Longitudinal Stream Profiles in Virginia and Maryland: USGS Professional Paper, v. 294-B, p. 45-97.
Hartley, A.J., and Chong, G., 2002, Late Pliocene age for the Atacama Desert: Implications for the desertification of western South America: Geology, v. 30, p. 43-46.
Hartley, A.J., Mather, A. E., Jolley, E., Turner, P., , 2005, Climatic controls on alluvial-fan activity, Coastal Cordillera, northern Chile, Alluvial Fans: Geomorphology, Sedimentology, Dynamics: Geological Society, London, Special Publications, v. 251, p. 95-115.
Hooke, R.B., 1965, Alluvial Fans [Thesis thesis]: Pasadena, California Institute of Technology.
Hooke, R.L., and Rohrer, W.L., 1979, Geometry of Alluvial Fans - Effect of Discharge and Sediment Size: Earth Surface Processes and Landforms, v. 4, p. 147-166.
Houston, J., 2002, Groundwater recharge through an alluvial fan in the Atacama Desert, northern Chile: mechanisms, magnitudes and causes: Hydrological Processes, v. 16, p. 3019-3035.
—, 2006a, Evaporation in the Atacama Desert: An empirical study of spatio-temporal variations and their causes: Journal of Hydrology, v. 330, p. 402-412.
—, 2006b, The great Atacama flood of 2001 and its implications for Andean hydrology: Hydrological Processes, v. 20, p. 591-610.
Keller, G., Adatte, T., Hollis, C., Ordonez, M., Zambrano, I., Jimenez, N., Stinnesbeck, W., Aleman, A., and HaleErlich, W., 1997, The Cretaceous/Tertiary boundary event in Ecuador: reduced biotic effects due to eastern boundary current setting: Marine Micropaleontology, v. 31, p. 97-133.
Kober, F., Ivy-Ochs, S., Schlunegger, F., Baur, H., Kubik, P.W., and Wieler, R., 2007, Denudation rates and a topography-driven rainfall threshold in northern Chile: Multiple cosmogenic nuclide data and sediment yield budgets: Geomorphology, v. 83, p. 97-120.
Lamy, F., Hebbeln, D., and Wefer, G., 1999, High-resolution marine record of climatic change in mid-latitude Chile during the last 28,000 years based on terrigenous sediment parameters: Quaternary Research, v. 51, p. 83-93.
Limerinos, J.T., 1970, Determination of the Manning coefficient from measured bed roughness in natural channels: U.S. Geological Survey Water-Supply Paper, v. 1898-B, p. 47.
McKay, C.P., Friedmann, E. I., Gómez-Silva, B., Cáceres-Villanueva, L., Andersen, D. T., Landheim, R., 2003, Temperature and Moisture Conditions for Life in the Extreme Arid Region of the Atacama Desert: Four Years of Observations Including the El Niño of 1997–1998: Astrobiology, v. 3, p. 393-406.
Milana, J.P., and Ruzycki, L., 1999, Alluvial-fan slope as a function of sediment transport efficiency: Journal of Sedimentary Research, v. 69, p. 553-562.

Nishiizumi, K., Caffee, M.W., Finkel, R.C., Brimhall, G., and Mote, T., 2005, Remnants of a fossil alluvial fan landscape of Miocene age in the Atacama Desert of northern Chile using cosmogenic nuclide exposure age dating: Earth and Planetary Science Letters, v. 237, p. 499-507.

NRCS, 2005, WinTR-55 Users Manual, Volume 2009, Natural Resources Conservation Service.

O'Brien, J.S., Julien, P.Y., and Fullerton, W.T., 1993, Two dimensional water flood and mudflow simulation: Journal of Hydrologic Engineering, v. 119, p. 244-261.

Ortlieb, L., 1995, Eventos El Niño y episodios lluviosos en el Desiertode Atacama: el registro de los dos últimos siglos: Bulletin de l'Institut Français d' Etudes Andines, v. 24, p. 519-537.

Pardocasas, F., and Molnar, P., 1987, Relative Motion of the Nazca (Farallon) and South-American Plates since Late Cretaceous Time: Tectonics, v. 6, p. 233-248.

Parker, G., Klingeman, P. C., and McLean, D. G., , 1982, Bed load and size distribution in paved gravel-bed streams: Journal of Hydraulic Engineering-Asce, v. 108, p. 544-571.

Parker, G., Paola, C., Whipple, K.X., Mohrig, D., Toro-Escobar, C.M., Halverson, M., and Skoglund, T.W., 1998, Alluvial fans formed by channelized fluvial and sheet flow. II: Application: Journal of Hydraulic Engineering-Asce, v. 124, p. 996-1004.

Pelletier, J.D., Mayer, L., Pearthree, P.A., House, P.K., Demsey, K.A., Klawon, J.E., and Vincent, K.R., 2005, An integrated approach to flood hazard assessment on alluvial fans using numerical modeling, field mapping, and remote sensing: Geological Society of America Bulletin, v. 117, p. 1167-1180.

PSD, N.O.E., 2009, NCEP Reanalysis data, Volume 2009: Boulder, CO.

Riquelme, R., Martinod, J., Herail, G., Darrozes, J., and Charrier, R., 2003, A geomorphological approach to determining the Neogene to Recent tectonic deformation in the Coastal Cordillera of northern Chile (Atacama): Tectonophysics, v. 361, p. 255-275.

Shields, A., 1936, Anwendung Aenlich Keitsmechanik und der Trubulenzfor-schung auf Die Geschiebebewegung: Schiffbau, Berlin, Germany, Mitteilungen de Preussischen Versuchsanstalt fur Wasserbau und Schiffbau.

Stelczer, K., 1981, Bed Load Transport: Littleton, Colorado: Water Resources Publications, p. 295 p.

Stock, J.D., Schmidt, K.M., and Miller, D.M., 2008, Controls on alluvial fan long-profiles: Geological Society of America Bulletin, v. 120, p. 619-640.

Strand, R.I., 1973, Sedimentation, Design of small dams: Washington D.C., U.S. Bureau of Reclamation, p. 767-796.

Thiel, M., Macaya, E.C., Acuna, E., Arntz, W.E., Bastias, H., Brokordt, K., Camus, P.A., Castilla, J.C., Castro, L.R., Cortes, M., Dumont, C.P., Escribano, R., Fernandez, M., Gajardo, J.A., Gaymer, C.F., Gomez, I., Gonzalez, A.E., Gonzalez, H.E., Haye, P.A., Illanes, J.E., Iriarte, J.L., Lancellotti, D.A., Luna-Jorquerai, G., Luxoroi, C., Manriquez, P.H., Marin, V., Munoz, P., Navarrete, S.A., Perez, E., Poulin, E., Sellanes, J., Sepulveda, H.H., Stotz, W., Tala, F., Thomas, A., Vargas, C.A., Vasquez, J.A., and Vega, J.M.A., 2007, The Humboldt Current System of northern and central Chile: Oceanography and Marine Biology, Vol 45, v. 45, p. 195-344.

USDA, 1986, Small Watershed Hydrology (WinTR-55 Model, USDA Agricultural Reserach Service.

Vargas, G., Rutllant, J., and Ortlieb, L., 2006, ENSO tropical-extratropical climate teleconnections and mechanisms for Holocene debris flows along the hyperarid coast of western South America (17 degrees-24 degrees S): Earth and Planetary Science Letters, v. 249, p. 467-483.

Volker, H.X., Wasklewicz, T.A., and Ellis, M.A., 2007, A topographic fingerprint to distinguish alluvial fan formative processes: Geomorphology, v. 88, p. 34-45.

Wilcock, P.R., 2001, Toward a practical method for estimating sediment-transport rates in gravel-bed rivers: Earth Surface Processes and Landforms, v. 26, p. 1395-1408.

Willmott, C.a.M., K.,, 1999, University of Delaware Air Temperature and Precipitation.

8 Figures and tables

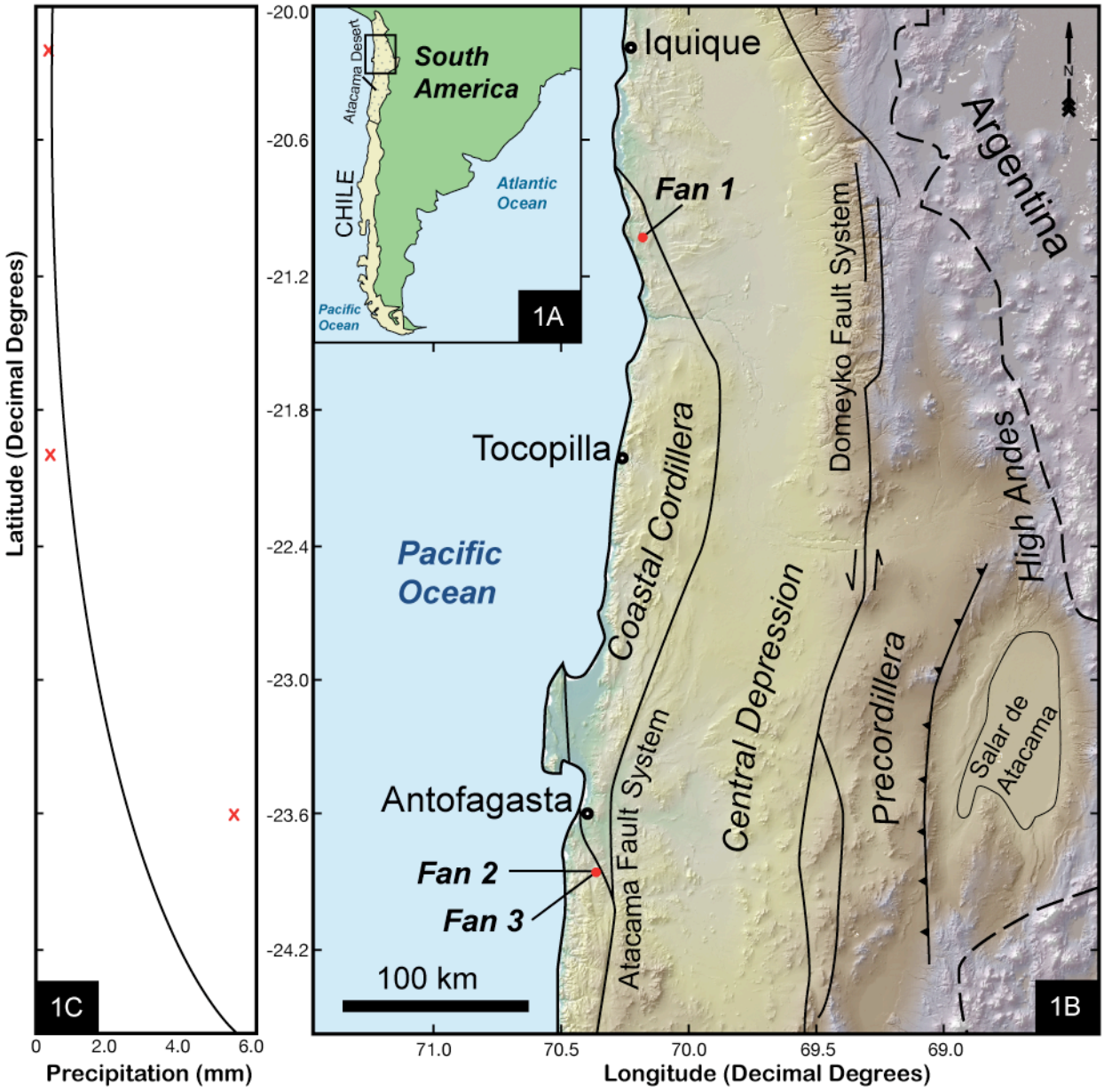

Figure 1. *Central Atacama Desert. (A) Generalized map of southern South America with the Atacama Desert of Chile shown. Coastal upwelling of cold Pacific waters from the south exerts a strong control on the climate by reducing the uptake of moisture along the coast. (B) Regional map of the central Atacama Desert (area outlined in Fig. 1A). Major cities, physiographic provinces, and tectonic structures are shown along with the locations of fans 1-3. Note the proximity of fans 1-3 to the Atacama Fault System (AFS). Shaded relief base image from ASTER; resolution 30m/px. (C) Average annual precipitation vs. latitude for the study area at the coastal cities Iquique, Tocopilla, and Antofagasta (Fig. 1B) showing an exponential decrease in precipitation to the north (data from (Vargas et al., 2006); (Ortlieb, 1995)). Precipitation increases systematically with increasing elevation to the east (Houston, 2002, 2006b).*

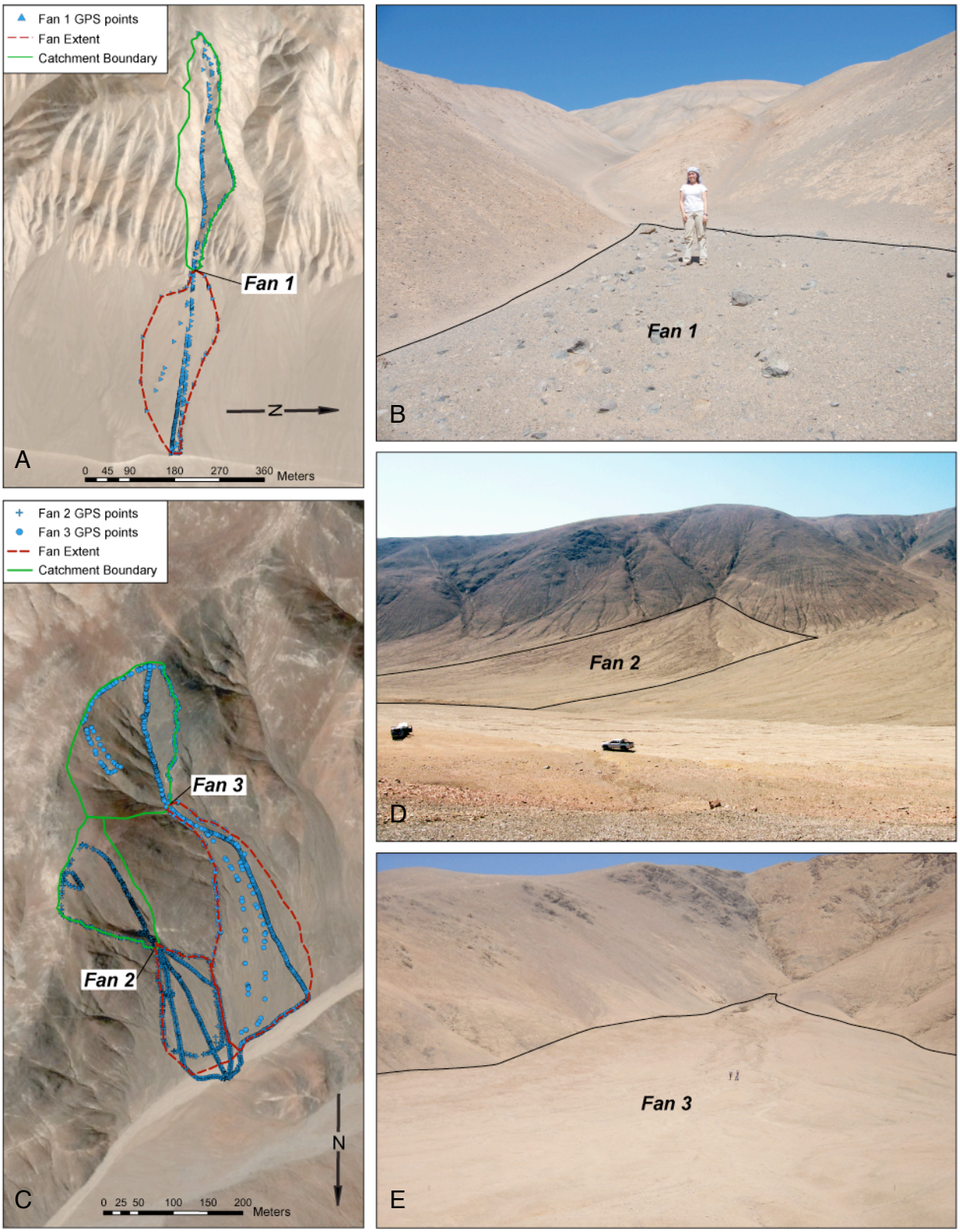

Figure 2. *Study area photographs and data coverage. Fan 1 is formed from a north-striking linear ridge ~400 km north of Antofagasta. (A) Aerial photograph of Fan 1. Note the narrow catchment from which the fan is formed. Data Coverage for Fan 1 shown from Differential GPS measurements. Catchment and fan are delineated for reference. (B) Field photo showing the large d95 clasts proximal to the apex of Fan 1 (person for scale). (C) Aerial photograph showing Fans 2 and 3 emerging NW from their catchments where their toe is cut by an axial channel (~2 m deep). Data Coverage for Fans 2 and 3 shown from Differential GPS measurements. Catchments and fans are delineated for reference. (D) Field photo of Fan 2 (vehicle for scale). (E) Field photo of Fan 3 looking up-fan (SE).*

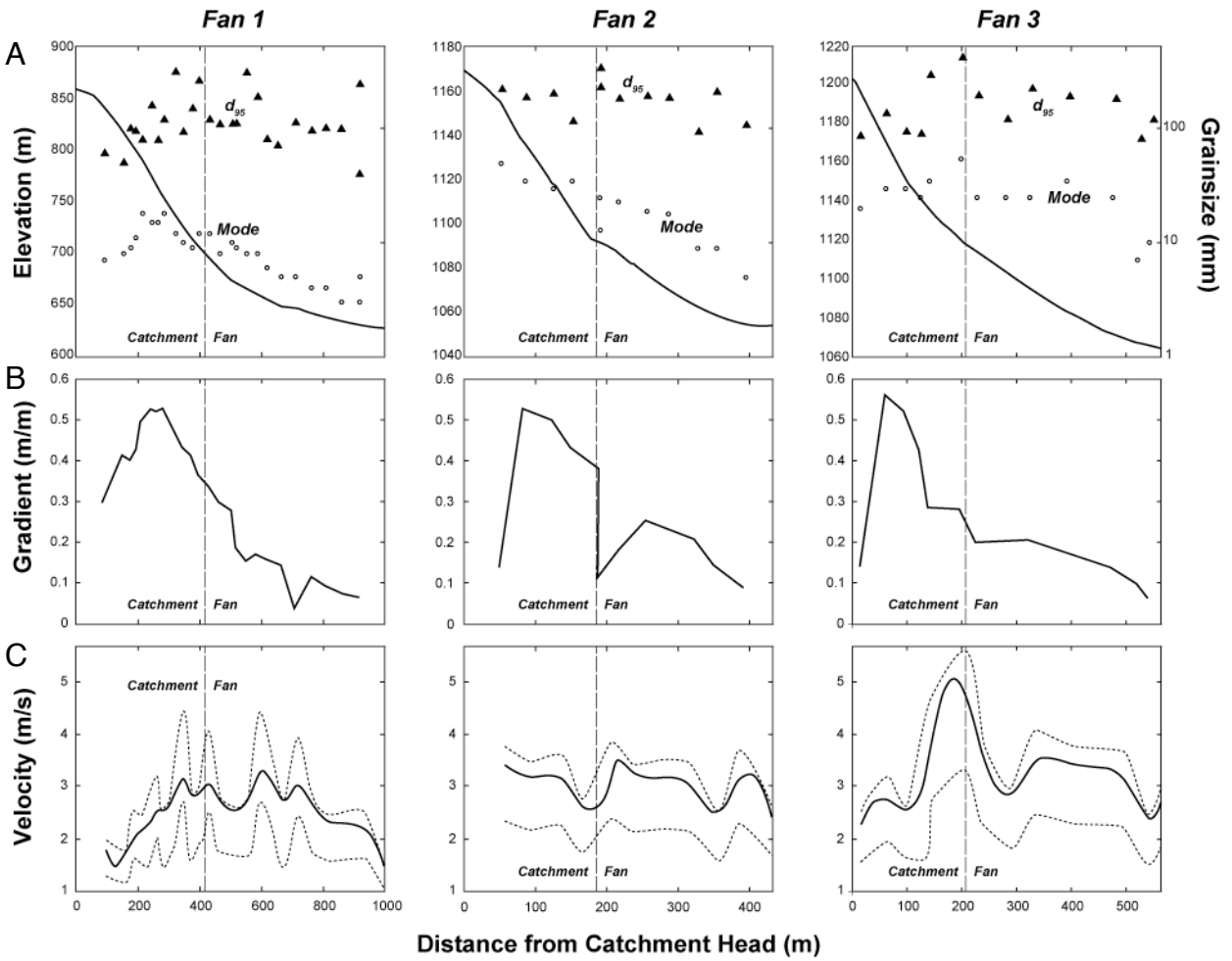

Figure 3. *Elevation Profiles, grain sizes, slope, and reconstructed entrainment velocities. (A) Plots showing the slope each fan and associated d_{md} and d_{95} grain sizes. Note the high variability of d_{95} clasts with distance when compared to the relatively more predictable decrease in mode grain size. (B) Slopes plotted with distance along profile for fans 1-3. (C) Reconstructed flow velocities for Fans 1-3 showing the velocity estimates calculated for each catchment and fan with respect to distance from the upper catchment boundary (along the main profile). Note the increasing trend in the catchment that transitions to a decreasing trend on the fan surface. This indicates that grain sizes are decreasing on the fan surface faster than the slope, meaning that lower flow rates can transport distal materials.*

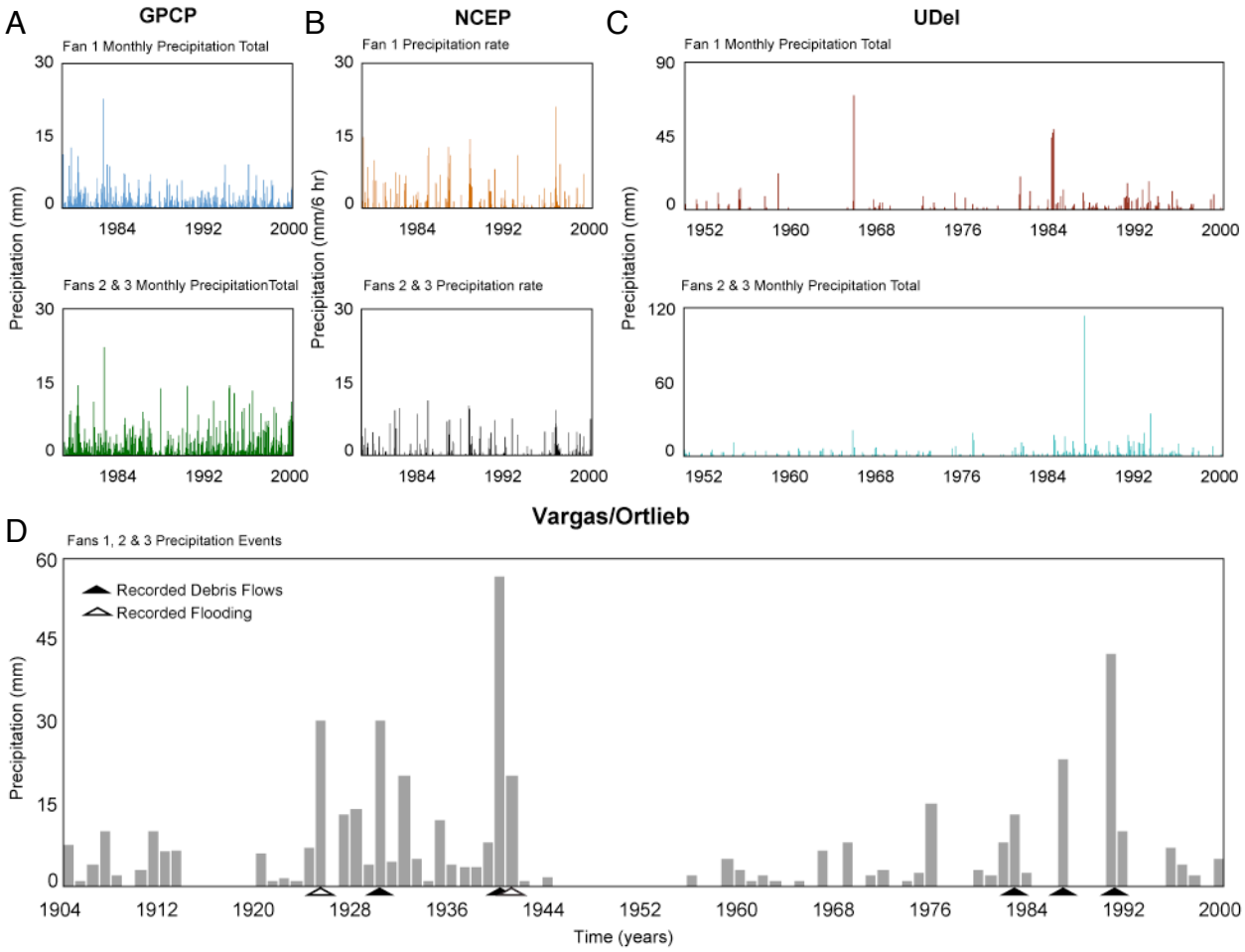

Figure 4. *Precipitation records for Fans 1-3. (A) Satellite derived GPCP monthly precipitation totals from 1979-2000 (Adler, 2003). (B) NCEP 6-hourly precipitation rate records from reanalysis from 1979-2000 (Kalnay et al., 1996). (C) Historically observed data from the University of Delaware (UDel) 1950-2000 (Legates, 1990; Shepard, 1968; Willmott, 1995; Willmott, 1985). (D) Combined plot of data from Vargas (2006) and Ortlieb (1995) for Antofagasta and Iquique 1904-2000. Triangles mark recorded instances of debris flows and flooding. Note differences in precipitation totals and timing for each dataset.*

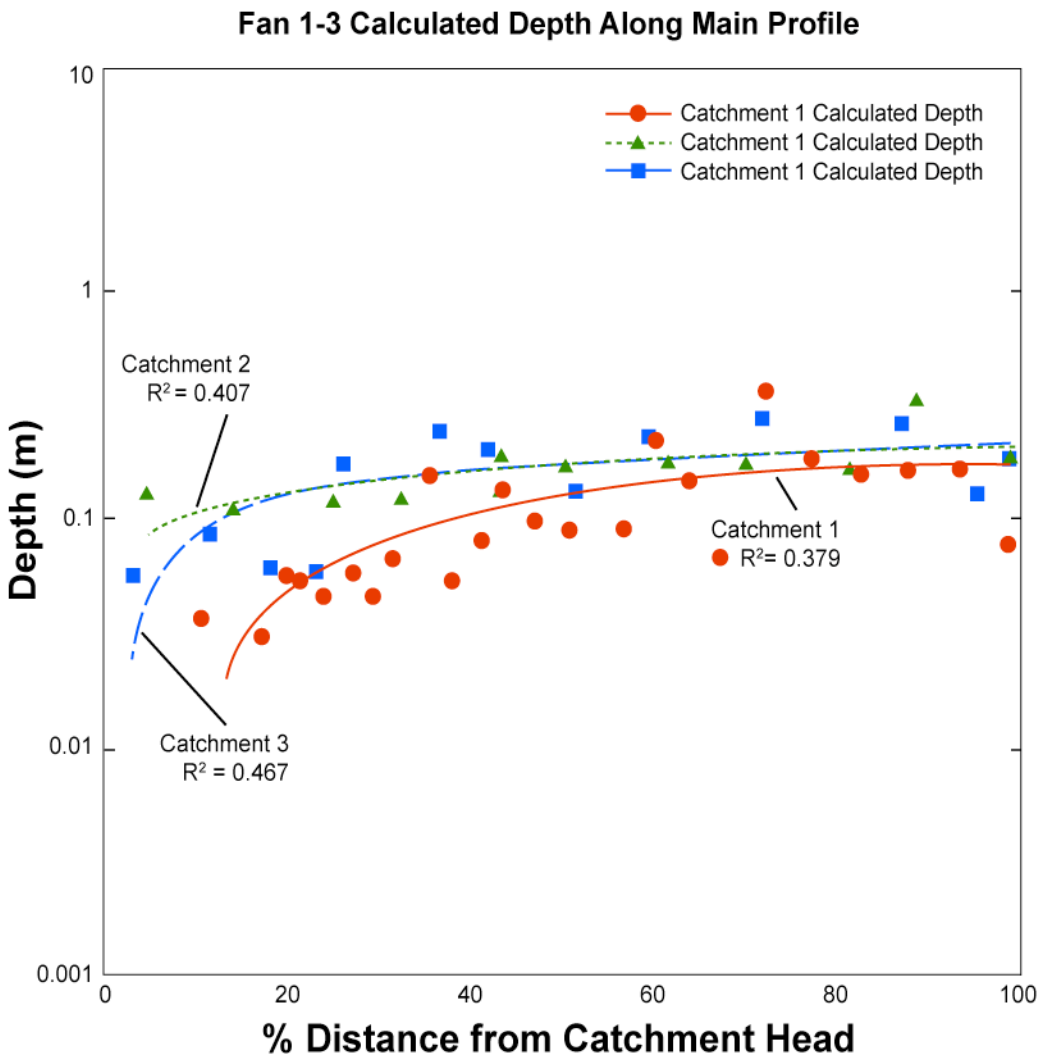

Figure 5. *Calculated minimum depth of flow along profile for fans 1-3. Plot shows that while depths vary greatly towards the catchment boundary --or divide, they conform to a similar value and slope down catchment. Trend lines are present for illustration purposes only. Depth of flow required to form fan 1 is less than fans 2 and 3 which are separated from fan 1 by ~400 km*

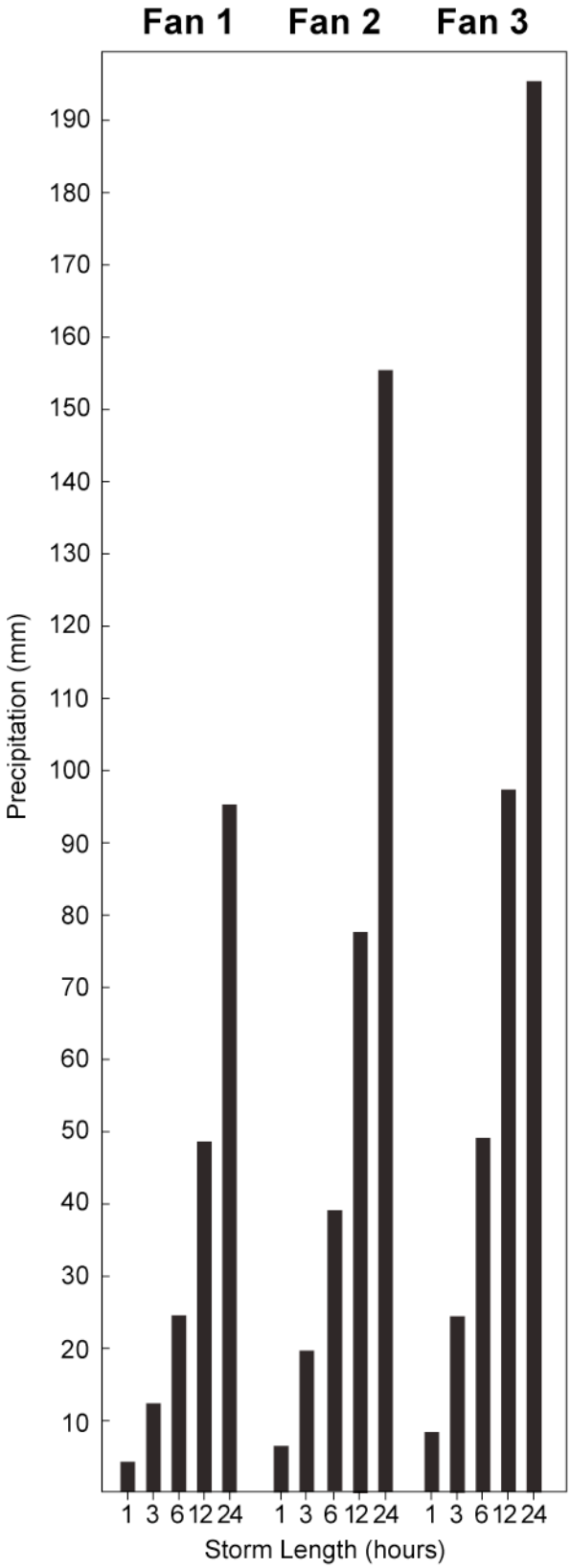

Figure 6. *WinTR-55 results for storm runoff reconstructions. The WinTR-55 model was evaluated for 1, 3, 6, 12, and 24 hour storm durations. The vertical bars represent minimum precipitation totals over those intervals required to mobilize the largest particles on each fan/catchment system. Note that fan 1 requires the least precipitation to "activate" the surface (4.04 mm/hr) vs. southern fans proximal to Antofagasta (6.46 and 8.13 mm/hr respectively). Bars are 1:1 scale.*

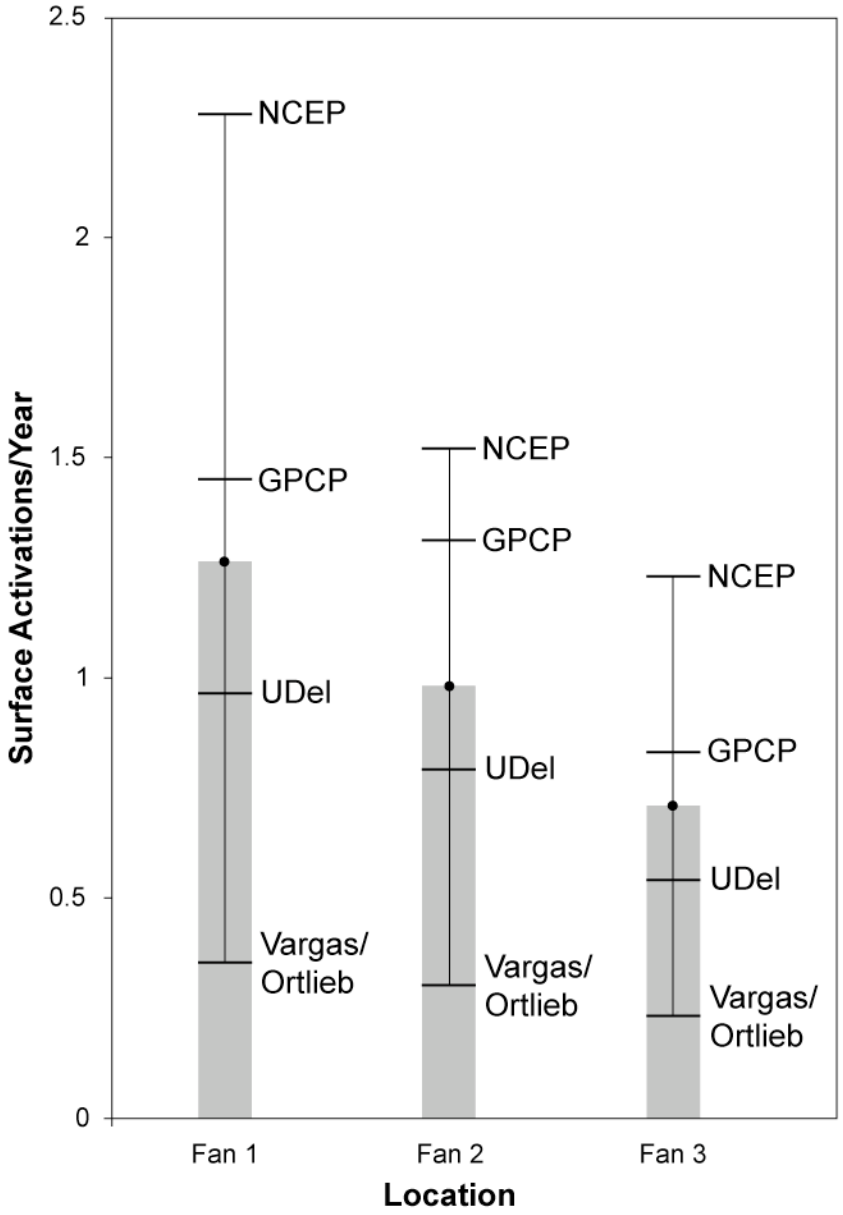

Figure 7. *Surface activation frequencies. Grey bars represent the means of the four datasets shown above. Frequencies calculated by summing the number of events that have exceeded necessary runoff thresholds (Fig 6.) for each dataset for the interval 1979-2000 since all datasets share that time coverage. Note that Vargas/Ortlieb likely underestimates the recurrence of surface forming flows due to point sourced data while NCEP/NCAR reanalysis over-estimates activation when compared to the mean of all dataset predictions. GPCP and UDel most closely approximate the mean of all data analyzed.*

Table 1 - Fan/Catchment Characteristics and Associated Flow Reconstruction Results

A **Fan Characteristics**

	Fan 1	Fan 2	Fan 3
Area (km^2):	0.045	0.017	0.031
Radius (m):	395.7	201.1	339.4
Avg. Slope (m/m):	0.138	0.198	0.206
Max Slope (m/m):	0.249	0.404	0.364
Avg. Profile Slope (m/m):	0.297	0.266	0.252
Avg. d95 (mm):	131.3	192.9	202.6
Avg. mode (mm):	9.2	22.6	26.7

B **Catchment Characteristics**

	Fan 1	Fan 2	Fan 3
Area (km^2):	0.04	0.02	0.03
Main Stream Length (m):	565.38	255.89	210.22
Avg. Slope (m/m):	0.329	0.321	0.245
Max Slope (m/m):	0.445	0.404	0.364
Avg. Profile Slope (m/m):	0.4489	0.50205	0.49833
Avg. d95 (mm):	130.0	220.8	220.8
Avg. mode (mm):	12	31.33	32.5
Aspect Ratio (m/m):	0.40	0.46	0.59

C **Model Results:**

	Fan 1	Fan 2	Fan 3
Bradley & Mears Bed Velocity (m/s)	2.756	3.408	3.426
Costa's Bed Velocity (m/s)	1.871	2.302	2.312
Least Squares Regression (m/s)	1.779	2.162	2.168
Strand's Bed Velocity (m/s)	2.066	2.555	2.568
Average Flow Velocity (m/s)	2.542	3.128	3.142
Manning's Flow Depth (m)	0.154	0.189	0.196
Shield's Depth (m)	0.008	0.010	0.011
Limerinos Depth (m)	0.165	0.262	0.276
Average Flow Depth (m)	0.109	0.154	0.161
Average Discharge (m^3/s):	0.081	0.129	0.175

Table 2 - One-Dimensional Flow Modeling Units and Equations

Symbol	Unit	Value	Description
$\mathbf{d}$	(m)	Measured	Distance from catchment head
$\mathbf{h}$	(m)	Measured	Elevation above sea level
$\mathbf{S}$	(m/m)	Measured	Slope
$\mathbf{d_i}$	(mm)	Measured	Sampled d_{95} grain size
$\mathbf{d_{md}}$	(mm)	Measured	Sampled mode grain size
$\boldsymbol{\gamma_s}$	(kg/m^3)	25970	Sediment density
$\boldsymbol{\gamma_f}$	(kg/m^3)	9800	Fluid density (water)
$\mathbf{g}$	(m/s^2)	9.8	Acceleration due to gravity
$\boldsymbol{\mu}$	-	0.7	Coefficient of static friction
$\mathbf{C_L}$	-	0.178	Lift Coefficient
$\mathbf{C_D}'$	-	0.1875	Drag Coefficient
$\mathbf{n}$	-	0.05	Manning's 'n'
$\boldsymbol{\omega}$	(N/m/s)	$0.009\mathbf{d_i}^{1.686}$	Unit Stream Power (Bagnold, 1966)
$\boldsymbol{\tau}$	(N/m^2)	$0.163\mathbf{d_i}^{1.213}$	Shear stress regression (Costa, 1983)
$\boldsymbol{\tau^*}$	-	$\boldsymbol{\tau}/[\mathbf{d_i}(\boldsymbol{\gamma_s}-\boldsymbol{\gamma_f})]$	Dimensionless shear stress
$\mathbf{v_{bb}}$	(m/s)	$[\{2(\boldsymbol{\gamma_s}-\boldsymbol{\gamma_f})\mathbf{d_I g \mu}\}/\{\boldsymbol{\gamma_f}^*(\mathbf{CL}+\mathbf{C_D})\}]^{0.5}$	Minimum bed velocity (Bradley & Mears, 1980)
$\mathbf{v_{bc}}$	(m/s)	$0.18\mathbf{d_i}^{0.487}$	Minimum bed velocity (Costa, 1983)
$\mathbf{v_{bl}}$	(m/s)	$0.2\mathbf{d_i}^{0.455}$	Least Squares Velocity (Costa, 1983)
$\mathbf{v_{bs}}$	(m/s)	$5.9\mathbf{d_i}^{0.5}$	Minimum bed velocity (Strand, 1973)
$\mathbf{v_{avg.}}$	(m/s)	$[1.2(\mathbf{v_{bb}}+\mathbf{v_{bc}}+\mathbf{v_{bl}}+\mathbf{v_{bs}})]4$	Depth averaged velocity
$\mathbf{D_m}$	(m)	$[(\mathbf{vn})/\mathbf{S}^{0.5}]^{1.5}$	Manning's depth
$\mathbf{D_b}$	(m)	$\boldsymbol{\omega}/(\boldsymbol{\gamma_f}\mathbf{S}\mathbf{v_{avg}})$	Bagnold stream power derived depth
$\mathbf{D_s}$	(m)	$[\boldsymbol{\tau}\mathbf{d_i}(\boldsymbol{\gamma_s}-\boldsymbol{\gamma_f})]/(\boldsymbol{\gamma_f}\mathbf{S})$	Shield's depth
$\mathbf{D_l}$	(m)	$\mathbf{v}/(8\mathbf{DgS})^{0.5}=1.16+2.03\log(\mathbf{D}/\mathbf{d_i})$	Limerinos depth
$\mathbf{D_{avg.}}$	(m)	$(\mathbf{D_m}+\mathbf{D_b}+\mathbf{D_s}+\mathbf{D_l})/4$	Average depth
$\mathbf{S_t}$	(m/m)	$\tan[\theta(\pi/180)]$	Slope transverse to channel
$\mathbf{A}$	(m^2)	$\mathbf{D}[\mathbf{D}/\tan(\mathbf{S_t})]$	Channel area
$\mathbf{Q}$	(m^3/s)	$\mathbf{Av_{avg.}}$	Depth averaged discharge

Table 3 - Precipitation Thresholds and Activation Frequencies per Dataset

Surface Activation Thresholds

	Discharge (m^3/s)	Precipitation rate to generate Q (mm/hr)
Fan 1	0.08	4.04
Fan 2	0.129	6.46
Fan 3	0.175	8.125

Surface Activation: months activated/Dataset (1979-2000)

	GPCP (1979-2000)	NCEP (1979-2000)	UDEL (1979-2000)	VARGAS/ORTLIEB (1979-2000)
Fan 1	33	48	33	7
Fan 2	24	32	29	6
Fan 3	15	26	23	5

Surface Activations/Year

	GPCP (1979-2008)	NCEP (1979-2000)	UDEL (1948-2000)	VARGAS/ORTLIEB (1904-2000)
Fan 1	1.45	2.28	0.96	0.35
Fan 2	1.31	1.52	0.79	0.30
Fan 3	0.83	1.23	0.54	0.23